

Superior damage tolerance of fish skins

Emily Zhang¹, Chi-Huan Tung², Luyi Feng³, Yu Ren Zhou^{2,*}

¹State College Area High School, State College, PA 16801

²Department of Materials Science and Engineering, Massachusetts Institute of Technology,
Cambridge, MA 02139

³Department of Engineering Science and Mechanics, The Pennsylvania State University, PA,
16802

*Corresponding author: wyrzhou@alum.mit.edu

Abstract

Skin is the largest organ of many animals. Its protective function against hostile environments and predatorial attack makes high mechanical strength a vital characteristic. Here, we measured the mechanical properties of bass fish skins and found that fish skins are highly ductile with a rupture strain of up to 30-40% and a rupture strength of 10-15 MPa. The fish skins exhibit a strain-stiffening behavior. Stretching can effectively eliminate the stress concentrations near the pre-existing holes and edge notches, suggesting that the skins are highly damage tolerant. Our measurement determined a flaw-insensitivity length of several millimeters, which exceeds that of most engineering materials. The strain-stiffening and damage tolerance of fish skins are explained by an agent-based model of collagen network in which the load-bearing collagen microfibers assembled from nanofibrils undergo straightening and reorientation upon stretching. Our study inspires development of artificial skins that are thin, flexible, but highly fracture-resistant and widely applicable in soft robots.

1. Introduction

Skin is a multifunctional organ that provides protection to animals from their living environment by regulating body temperature and sensing external stimuli¹. Skin is made of three layers: epidermis, the top layer; dermis, the middle layer; and hypodermis, the bottom layer¹. The epidermis is the water-resistant outer layer of skin and the body's first line of defense against environmental attacks, ultraviolet radiation, bacteria, and other pathogens. It is also responsible for cell renewal. The dermis is responsible for the structure and mechanical properties of skin and mostly composed of the proteins collagen and elastin. Collagen is the major load-bearing structure^{2,3}, while elastin provides flexibility for the skin⁴. The lower layer of the dermis, the stratum compactum, consists of a orthogonal cross-ply arrangement of collagen microfibers with well-defined angles ($\sim 40^\circ$ - 60°) relative to the long axis (length) of the fish⁵. The hypodermis is the layer of skin where fat is deposited and stored. The presence of multiple layers allows the skin to achieve many functions.

Robust mechanical properties of skin are essential to ensure its function as a self-healing protective layer after being subject to mechanical loads such as abrasion and tearing. The skins of different animals have been studied⁶⁻⁹, which are often considered to be nonlinearly elastic. Far less is known about the plasticity and damage tolerance of skin. Because skin is a polymeric structure with a hierarchical order^{4,8}, plastic deformation likely originates from the rearrangement of the collagen microfibril network rather than dislocation motion, which often occurs in metals.

In this study, we characterize the mechanical properties of fish skins under tensile loading. Our measurements show that fish skin is highly ductile, nonlinear, and exhibits a strain-stiffening behavior. Loading and unloading cycles show that fish skin undergoes large plastic deformation with significant hysteresis. Stretching can hardly lead to expansion of pre-cut holes and edge notches on the fish skin; instead, stretching effectively eliminates the stress concentration near the defects, demonstrating that the skin is highly damage tolerant. Considering that the collagen

network is the major load-bearing structures in the skin, we develop an agent-based model of collagen network. Our agent-based simulations show that the superior mechanical properties of fish skins can be attributed to the rearrangement of the collagen microfibril network upon stretching.

2. Experimental investigation

2.1 Experimental procedures

Our apparatus setup included a MARK-10 loading apparatus and force gauge, optical microscope, and specimen samples. Fresh striped bass fish were acquired from a local fish store (Cambridge, MA). The fish were about ~20 cm in length and ~8 cm in width and kept hydrated on ice before sample collection. Sample collection was conducted within a few hours of purchasing. Two rectangular tissue samples of ~5-7 cm length and ~2-3 cm width running from anterior to posterior of each fish was then extracted, one sample from each side of a fish. Flesh attached to the bottom surface of each rectangular tissue sample was carefully removed. The thickness of the obtained skin sample was ~0.3 mm. Strips of 1 cm width and ~5-7 cm length were then cut parallel to each other from this skin sample. These 1 cm-wide strips were tensile test samples, with the loading axis parallel to the length. The in-plane collagen fibril orientations relative to the tensile axis were the same (~40°-60°) for all the samples⁵. In total, three fish of similar size were used, and each fish provided six 1 cm-wide test samples. The samples were kept hydrated with fresh water between sample collection and tensile testing.

During tensile testing, the strips were clamped to the testing apparatus with a grip at each end, and uniaxial tension was applied along the length direction until the strips ruptured. For each specimen, the stretch rate was kept at 10 mm/min. The stress is calculated by $\sigma = F/(wt)$, where w is the width and t is the thickness. The engineering strain is calculated by $\varepsilon = \Delta l/l_0$, where the elongation is $\Delta l = l - l_0$, and l and l_0 are the stretched and original lengths of the specimen, respectively. The stretched length was calculated by multiplying the grip-grip displacement rate

by the elapsed time. As the strain calculation was based on the recorded grip-grip displacement, sample-grip slip may cause strain measurement inaccuracy. However, the error due to sample-grip slip is negligible in our experiments. The fish skin samples in our experiments reach a grip-grip displacement of a few-cm before rupture occurs, whereas the sample-grip slip that we observed was at most a few-mm. The different orders of magnitude of the displacement and slip gives us great confidence in our strain measurements.

2.2 Tensile response of fish skin

We performed several tensile tests with the fish skin samples. A typical stress/strain relation is shown in **Fig. 1**. The stress-strain relation is highly nonlinear. The stiffness of the skin – the slope of the stress-strain curve – increases with strain, indicating a strain-stiffening effect. The infinitesimal Young's modulus of the fish skin is roughly 13.3 MPa at 0% strain, but can reach as high as 54.4 MPa at 20% strain. The fish skin is highly extensible with a rupture strain of nearly 30%. The tensile strength of the skin can reach 14 MPa. From our experiments, failure often occurs near the clamped ends of the testing samples, but rarely in the center, possibly due to stress localization at the clamped ends. Therefore, fish skin specimens with more optimized geometries which reduce stress localization at the clamped ends may exhibit even higher tensile strength. The fish skin samples were not descaled since the natural tensile response of the skin was of interest in this study. It is known that scales provide out-of-plane puncture resistance of the skin⁵. Scales also influence tensile response significantly. The tensile specimen can be decomposed into scaled regions and non-scaled regions. Due to the much higher stiffness of the scaled regions relative to the non-scaled regions, strain is mainly localized at the non-scaled regions. Therefore, at a given stress, the local strain at non-scaled regions may be considerably higher than the strain measured in this study.

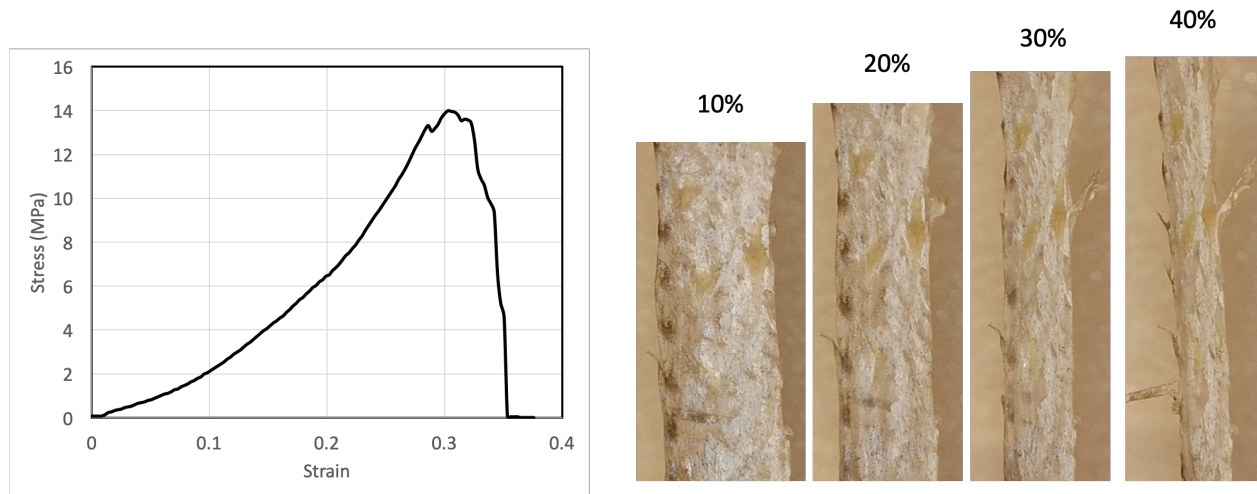


Fig. 1. A typical stress-strain relation of fish skins together with microscope images of the skin at selected tensile strains, showing that fish skin is highly extensible and strain stiffening.

2.3 Loading-unloading reveals strain-dependent mechanical properties

In real-life conditions, fish skins undergo frequent mechanical loading and unloading impacts, such as during cyclic motions of the fish's body. To study fish skins under mechanical cycling, we applied tensile loading and unloading cycles to the fish skin specimens. The specimens were first stretched to a certain force below the failure strength and then unloaded until the applied force returned to zero, then reloaded to a higher peak force until fracture occurred.

To see whether stretching may cause plastic deformation, we applied tensile loading-unloading cycles to the specimens (**Fig. 2**). For the first loading-unloading specimen, we unloaded the specimen to a 21% tensile strain (blue curve). Upon unloading to zero force, the specimen retained a plastic strain of 13.5%, suggesting an elastic strain of only 7.5% during loading. The large amount of plastic strain suggests permanent changes inside the skin. For metals and other crystalline materials, the unloading curve usually has the same slope as the elastic portion of the loading curve. However, for the fish skin, the unloading stiffness is much larger than the loading stiffness, indicating strain-dependent mechanical properties which may be due to microstructural changes during loading. The area encompassed by the loading and unloading curves is the energy

dissipated during the cycle. The significant hysteresis area in the stress-strain curve further indicates strain-dependent mechanical properties and microstructural rearrangement during loading. Reloading closely followed the previous elastic unloading curve until the previous maximal loading point was reached, showing that the mechanical properties do not change significantly during unloading-reloading steps up to the previous maximal point. Finally, continued loading beyond the previous maximal point leads to further plastic deformation.

For the second specimen, we conducted two loading-unloading cycles (orange curve). For this specimen, the initial Young's modulus was smaller than that of the first specimen, though strain-stiffening was observed for both specimens. Hysteresis occurred during both loading-unloading cycles. In each cycle, appreciable plastic deformation was generated in the tensile specimen. In the first cycle, the plastic strain was 14% with a total strain of about 19%, suggesting an elastic strain of 5% built in the specimen during the first loading step. In the second cycle, the total strain (relative to after the first unloading) was 10% and the plastic strain generated was about 3%, leading to an elastic strain of 7%. Apparently, the plastic strain and hysteresis generated in the second cycle were markedly smaller than those in first cycle, possibly because of the strain-stiffening effect, making it increasingly more difficult to generate plastic deformation even at a higher applied load.

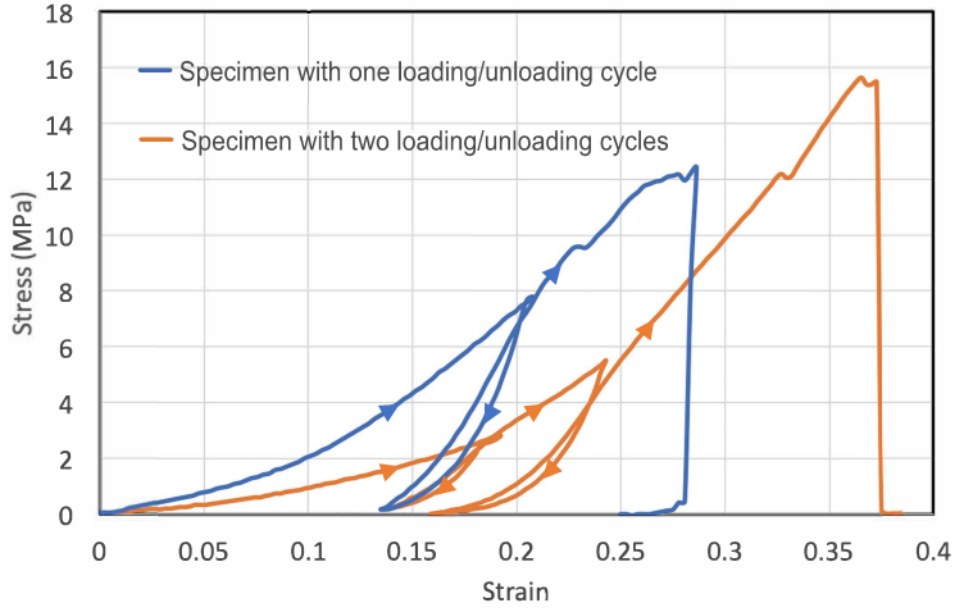


Fig. 2. Cyclic loading of the skin strips showing the large plastic deformation and significant hysteresis. The first specimen (blue) was subject to one loading/unloading cycle before reloaded to failure, whereas the second specimen (orange) was subject to two loading/unloading cycles. The loading/unloading directions are indicated by triangular arrows.

2.4 Slits and holes are insensitive to stretching

To test the fish skins' resistance to stress concentration rupture, we introduced holes to the specimens (**Fig. 3A**). The holes were irregular in shape but close to each other (**Fig. 3, A2**). In general, the presence of a hole causes stress concentration at the periphery of the hole, which then causes rupture of the ligament between the holes. The stress concentration scales with the equation $\alpha = 1 + \frac{2a}{b}$, where a is the radius of the hole along the width direction and b is the radius of hole in the length direction (stretching direction). For a circular hole, the stress concentration factor is 3. Unexpectedly, we found that stretching did not cause expansion of the holes or the rupture of the ligament between the holes. Instead, upon stretching, the holes were elongated along the stretching direction with increasing b but decreasing a (**Fig. 3, A2**). This significantly reduced the stress concentration factor α at the holes. In the end, the hole became a slit with $a \ll b$ and $\alpha \approx 1$,

which means a nearly eliminated stress concentration due to the hole geometry (Fig. 3, A3). Continuing stretching did cause rupture near the region where holes were introduced, probably due to reduced cross-section area. However, the failure strengths/strains were not significantly lower than the pristine specimens (**Fig. 3, A1**).

We also tested whether edge notches could cause significant damage to the skin (**Fig. 3B**). We introduced an edge notch to the specimens. The edge notches were about 5 mm-long, half of the width of the samples. We observed that during stretching the edge notch did not propagate as a crack. Instead, the notch became increasingly blunted and finally eliminated (**Fig. 3, B2-B3**). Necking then occurred at the blunted region and further stretching caused rupture in this region. There was no extension of the initial notch length. These experiments indicate that fish skins are highly tolerant to defects and mechanically very tough, a property which has previously been demonstrated in other materials^{10,11}.

To quantify the toughness, tensile tests of the notched and pristine specimens were carried out to determine the fracture energy of the fish skins^{12,13}. In each test, two specimens with the same dimensions were prepared and stretched; one was unnotched and the other was pre-notched. We stretched the unnotched specimen to rupture and determined the work of fracture, which is the area under the stress-stretch curve $w(\lambda)$, where $\lambda = \frac{l}{l_0} = 1 + \varepsilon$ is the mechanical stretch. λ_f is the stretch at which the unnotched sample ruptures. We then stretched the pre-notched specimen and found λ_c as the stretch at which the notched sample ruptures. Apparently, $\lambda_c < \lambda_f$. The fracture energy is then determined by $\Gamma = l_0 w(\lambda_c)$, where l_0 is the length of the skin strips in the undeformed state. For the first edge-notched specimen of initial length $l_0 = 7$ cm, $\lambda_c = 1.29$ (**Fig. 3, B1**), $w(\lambda_c)$ can be found from the strain-strain curve in Fig. 1 of the unnotched specimen. The fracture energy we measured was $\Gamma \sim 0.149$ MJ/m². The measured fracture energy (Γ) and the work of fracture of the unnotched sample ($w_f = w(\lambda_f)$) defines a characteristic length scale, $l_f = \Gamma/w_f$, termed as the flaw-sensitivity length¹² below which the stretchability of the skin is

insensitive to the flaw. For a pre-notch of length less than l_f , the notch has negligible effect on the critical stretch of the sample, and the sample is flaw insensitive; on the other hand, for a precut notch of length longer than l_f the notch significantly reduces the critical stretch of the sample. Our results show that the fracture toughness of the fish skins is $\sim 0.149 \text{ MJ/m}^2$ and the total work of fracture for a specimen without an initial cut is $\sim 2.45 \text{ MJ/m}^3$. This gives rise to a flaw-sensitivity length of $l_f \approx 6.1 \text{ mm}$, larger than that of most engineering materials¹². In light of the high flaw insensitivity of the fish skins, we expect that for sufficiently small notches of size less than l_f , the crack tip will first blunt and the notch will be eliminated upon further stretch, as seen in our experiments.

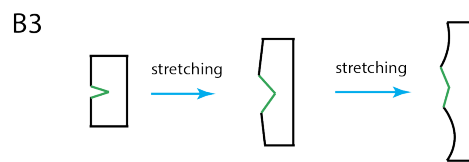
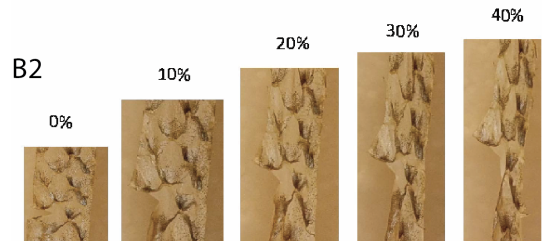
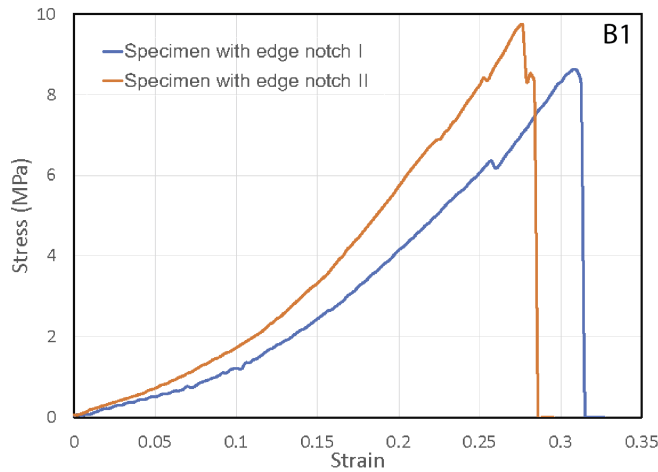
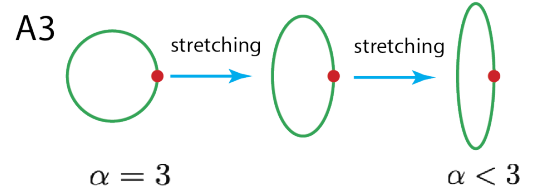
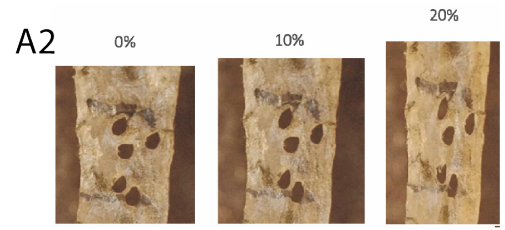
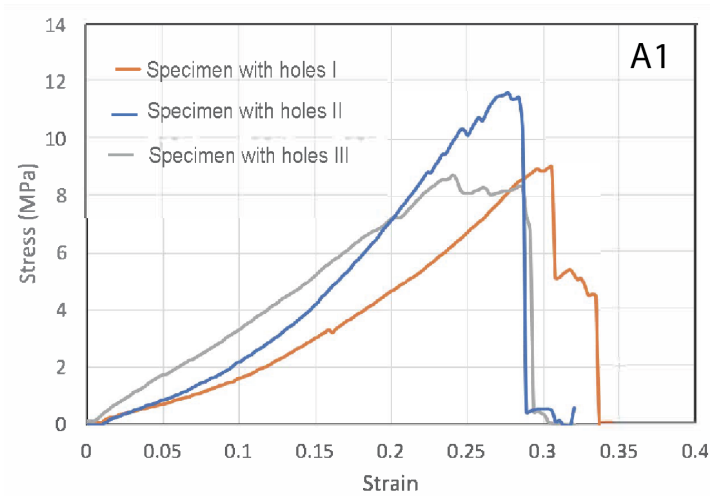


Fig. 3. Tear tests of fish skin strips with holes (**A1-A3**) and an edge notch (**B1-B3**). **A1.** Stress-strain curves of three specimens with pre-introduced holes. **A2.** The holes become elongated along the stretching direction, with a reduced stress concentration factor. **A3.** Schematics of the hole shape change due to stretching, resulting in reduced stress concentration factor. **B1.** Stress-strain curves of three specimens with a pre-introduced edge notch. **B2.** Under increasing stretch, the edge notch did not expand, but blunted. **B3.** A schematic illustration of the edge notch blunting due to stretching.

3. Agent-based modeling

3.1 Construction of an agent-based model

The primary load-bearing structure in fish skin is the collagen microfibril network^{3,8}, so a model of this network was constructed to better understand the mechanisms behind the experimental observations in the previous sections. In a natural, unstretched state, collagen nanofibrils are arranged to form thick collagen microfibers¹⁴, which adopt a roughly orthogonal cross-ply in-plane arrangement oriented 40°-60° with respect to the fish body length with some degree of waviness in the out-of-plane thickness direction⁵ (**Fig. 4A**). As such, our model is based on the in-plane orthogonal cross-ply arrangement and out-of-plane sinusoidal waviness of collagen microfibers in the unstretched state⁵, denoted here as a cross-helical structure. Each collagen microfiber was represented by a chain of beads, each bead having a diameter of $r_0 = 1 \mu\text{m}$ and mass of $m_0 = 7.01 \times 10^{-16} \text{ kg}$. A representative volume element (**Fig. 4B**) was chosen and periodic boundary conditions were applied at the sides of the element. To generate a cross-helical structure, collagen microfibrils were initially placed in two orthogonal orientations with a z-direction amplitude and wavelength of 5 and 100 μm respectively^{15,16}, and the dimensions of unit box were 70 $\mu\text{m} \times 70 \mu\text{m} \times 13 \mu\text{m}$.

The mechanical properties of collagen chains were determined by the interaction parameters,

including intra-fiber bond potential, intra-fiber angle potential, and inter-fiber interaction potential. These parameters were tuned to be consistent with Young's modulus, persistent length and adhesion energy, which have been measured experimentally. The intra-fiber bond potential within was described by a harmonic spring

$$U_{bond} = \frac{1}{2} k (r - r_0)^2$$

Where r is the distance between a pair of bonded beads, k is the spring constant and r_0 is the equilibrium bond length. The spring constant can be expressed by the Young's modulus E of the collagen fiber: $k = \frac{AE}{r_0}$, where A is the cross-section area of the microfibers. In our model, Young's modulus was given by $E = 6.5$ GPa, based on previous experimental work^{17,18}. The angle-bending potential is chosen to match the bending rigidity and persistence length of the collagen microfiber:

$$U_{angle} = \frac{l_p k_b T}{r_0} (1 + \cos(\theta))$$

Where l_p is the persistence length of the microfibers. Based on the published measurements¹⁸, the persistent lengths of collagen chain was set as 10 μm . The interaction between collagen beads from different fibers was described by the Lennard-Jones (LJ) potential¹⁹, where the energy parameter is set to be $\epsilon = 11$ kcal/mol.

All simulations were performed in LAMMPS. Starting with initial cross-helical configuration, simulations were performed for 1 ms using NVE ensemble and Langevin thermostat to maintain system temperature at 300 K until the system reached equilibrium. Then, an additional Berendsen barostat was applied to relax the stress for 100 μs . After the stress relaxation, the pre-equilibrated system was uniaxially stretched by deforming the simulation box along the stretching direction at a strain rate of 10^3 s^{-1} , with NVE ensemble and Langevin thermostat. The stretching direction was initially oriented at 45° with respect to the in-plane directions of the collagen microfibers.

3.2 Modeling results

We used the model to represent the fish skin and to compare its tensile response to the actual skin. The simulated stress-strain curve resembles our experimental data within 20% stretch (**Fig. 4, C1**).

A two-step stretching process was observed in our simulation. At smaller strains, the dominant mechanism was the reduction of out-of-plane waviness and straightening of the collagen microfibers (**Fig.4, C2**). At larger strains, the dominant mechanism switched to in-plane re-orientation of microfibers along the stretching direction (**Fig.4, C3**). As a result of this two-step stretching process, the collagen microfibers became increasingly aligned along the tensile axis, both in-plane and out-of-plane. These aligned microfibers can resist stretching more efficiently than those with the wavy morphology and larger orientation angles with respect to the tensile axis, which explains the strain-stiffening behavior. Straightening and reorientation are possibly both elastic and plastic, since part of the straightening and reorientation process may not be recoverable upon unloading, which contributes to plastic strain during stretching.

It should be noted that inter-fiber sliding of the aligned collagen microfibers may be a possible microfiber movement mode at relatively high stretch. Inter-fiber sliding usually occurs when the microfibers in contact are of different lengths or microfibers are broken during stretching. However, such microscopic structural information is currently not known from experimental imaging. The cross-ply arrangement may impose an interlocking effect that raises the energy required for inter-fiber sliding. Furthermore, inter-fiber sliding is of long range since one microfiber may be in contact with multiple microfibers, enabling long-range energy dissipation. Due to the use of periodic boundary conditions large-scale inter-fiber sliding is not simulated in our model. Nevertheless, the good agreement in the tensile response between our agent-based model and the experimental data indicates that fiber straightening and reorientation are the dominant modes in the range of the applied strain.

At the notch tip, all three elementary movements of collagen microfibers may be activated at small global strain because of the high stress concentration. Thus, the notch tip becomes more stiffened than other regions under the applied stretch, effectively avoiding further localized deformation and stress concentration at the notch tip. The local stiffening mechanism, combined with the long-

range energy dissipation of the collagen microfibers, explains the superior damage tolerance of fish skin.

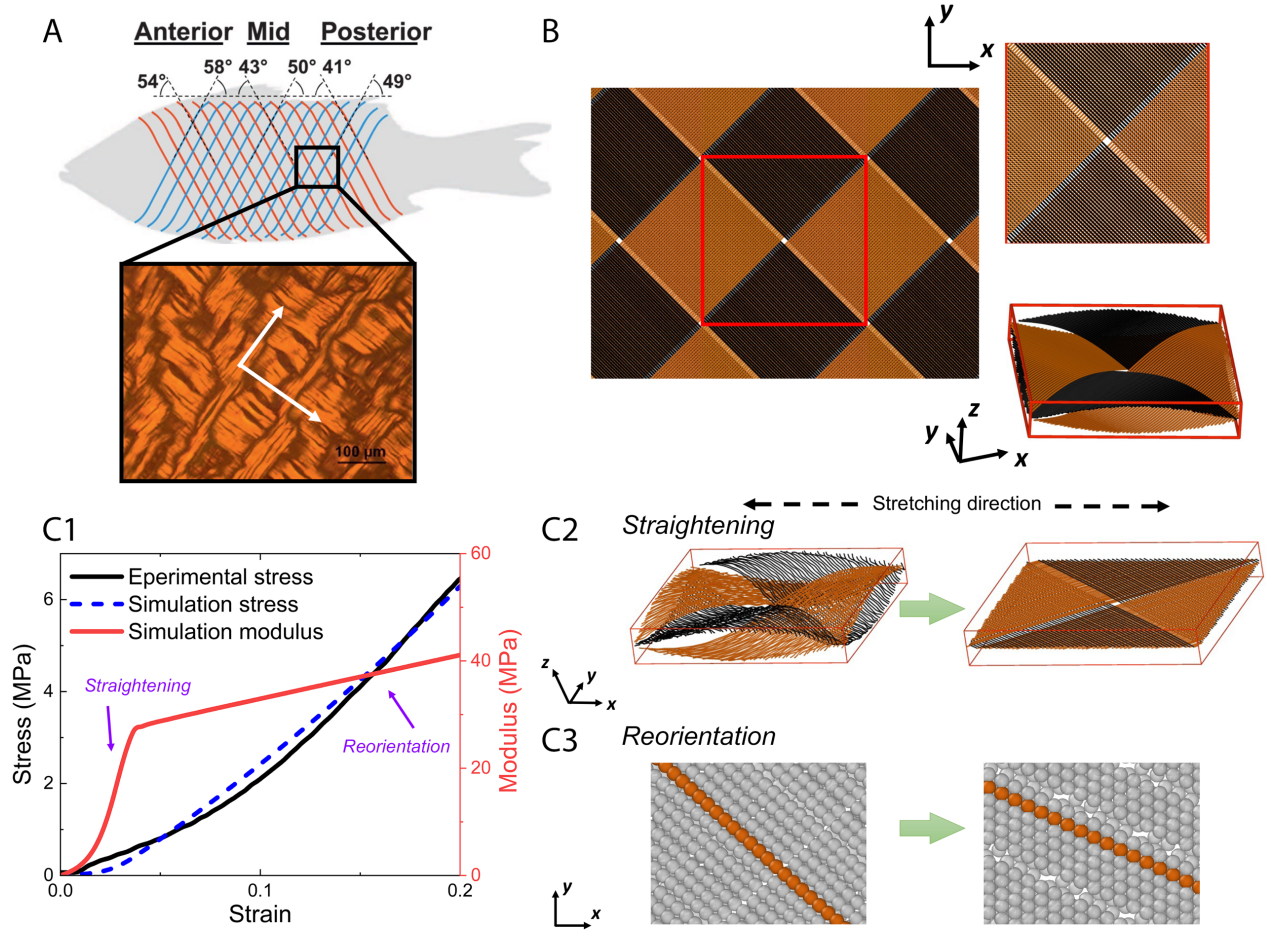


Fig. 4. The orthogonal-cross-ply structure of collagen microfibers in fish skin reproduced from reference⁵ (A), geometry setting of agent-based model (B), and tensile test results in simulation (C1-C3). (A) The periodic microfibers have two orthogonal principal directions. A corresponding representative volume element was generated (B), and then tensile test was applied. The stress-strain curve and modulus as a function of strain, from experimental and simulation (C1), show a two-step stretching process. Two primary movements, straightening (C2) and reorientation (C3) of the microfibers, dominate the tensile response successively, which together elucidate the

mechanism underlying strain-stiffening behavior of fish skin.

Conclusions

In summary, the mechanical properties of fish skins were characterized by testing skin strips in tension. We found that the fish skins become stiffer with stretching. More importantly, the fish skins are highly damage tolerant. This was demonstrated by the phenomena that stretching can eliminate the stress concentration near the holes and edge notches but cannot propagate or expand these defects. In particular, the flaw-sensitivity length for the fish skin was calculated to be ~6 mm, superior to most engineering materials. We attribute strain stiffening and the superior damage tolerance to the elementary collagen network movements, namely, microfiber straightening and reorientation, as verified by our agent-based modeling. The fundamental understanding of our study also provide guidance to the synthesis of multifunctional artificial skins²⁰ for soft robots that are mechanically robust and damage tolerant.

Acknowledgements

We thank Prof. Ju Li for his support and guidance on this research. Author contributions: E. Z.: experimental design, investigation, methodology, formal analysis, writing the original draft; C.-H. T.: Technical support and guidance; L. F.: agent-based modeling and data analysis; Y. Z.: Conceptualization, experimental design, supervision, writing, review, and editing.

Works cited

1. Jablonski, N. G. *Skin: a natural history*. (University of California Press, 2006).
2. Freed, A. D. & Doehring, T. C. Elastic model for crimped collagen fibrils. *J. Biomech. Eng.* **127**, 587–593 (2005).
3. Yang, W. *et al.* Protective role of Arapaima gigas fish scales: Structure and mechanical behavior. *Acta Biomater.* **10**, 3599–3614 (2014).
4. Oxlund, H., Manschot, J. & Viidik, A. The role of elastin in the mechanical properties of

- skin. *J. Biomech.* **21**, 213–218 (1988).
5. Szewciw, L. & Barthelat, F. Mechanical properties of striped bass fish skin: Evidence of an extensor function of the stratum compactum. *J. Mech. Behav. Biomed. Mater.* **73**, 28–37 (2017).
 6. Ridge, M. D. & Wright, V. The directional effects of skin. A bio-engineering study of skin with particular reference to Langer's lines. *J. Invest. Dermatol.* **46**, 341–346 (1966).
 7. Lanir, Y. & Fung, Y. C. Two-dimensional mechanical properties of rabbit skin-II. Experimental results. *J. Biomech.* **7**, (1974).
 8. Yang, W. *et al.* On the tear resistance of skin. *Nat. Commun.* **6**, 1–10 (2015).
 9. Ní Annaidh, A., Bruyère, K., Destrade, M., Gilchrist, M. D. & Otténio, M. Characterization of the anisotropic mechanical properties of excised human skin. *J. Mech. Behav. Biomed. Mater.* **5**, 139–148 (2012).
 10. Gao, H. & Chen, S. Flaw tolerance in a thin strip under tension. *J. Appl. Mech. Trans. ASME* **72**, 732–737 (2005).
 11. Gao, H., Ji, B., Buehler, M. J. & Yao, H. Mechanics of the 21st Century. *Mech. 21st Century* (2005) doi:10.1007/1-4020-3559-4.
 12. Chen, C., Wang, Z. & Suo, Z. Flaw sensitivity of highly stretchable materials. *Extrem. Mech. Lett.* **10**, 50–57 (2017).
 13. Zhang, W. *et al.* Fracture Toughness and Fatigue Threshold of Tough Hydrogels. *ACS Macro Lett.* **8**, 17–23 (2019).
 14. Gautieri, A., Vesentini, S., Redaelli, A. & Buehler, M. J. Hierarchical Structure and Nanomechanics of Collagen Microfibrils from the Atomistic Scale Up. *Nano Lett.* **11**, 757 (2011).
 15. Wang, B., Hua, Y., Brazile, B. L., Yang, B. & Sigal, I. A. Collagen fiber interweaving is central to sclera stiffness. *Acta Biomater.* **113**, 429–437 (2020).
 16. Gogola, A. *et al.* Spatial patterns and age-related changes of the collagen crimp in the human cornea and sclera. *Investig. Ophthalmol. Vis. Sci.* **59**, 2987–2998 (2018).
 17. Buehler, M. J. Nanomechanics of collagen fibrils under varying cross-link densities: Atomistic and continuum studies. *J. Mech. Behav. Biomed. Mater.* **1**, 59–67 (2008).
 18. Sivakumar, L. & Agarwal, G. The influence of discoidin domain receptor 2 on the persistence length of collagen type I fibers. *Biomaterials* **31**, 4802–4808 (2010).

19. Buehler, M. J. Atomistic and continuum modeling of mechanical properties of collagen: Elasticity, fracture, and self-assembly. *J. Mater. Res.* **21**, 1947–1961 (2006).
20. Yannas, I. V. & Burke, J. F. Design of an artificial skin. I. Basic design principles. *J. Biomed. Mater. Res.* **14**, 65–81 (1980).